SEM-ECC Investigation of Dislocation Arrangements in Cyclically Deformed Copper Single Crystals with Different Crystallographic Orientations

X.W.Li[1,2], Z.F.Zhang[1], Z.G.Wang[1], S.X.Li[1] and Y.Umakoshi[2]

[1] State Key Laboratory for Fatigue and Fracture of Materials, Institute of Metal Research, Chinese Academy of Sciences, Shenyang 110015, PR China

[2] Department of Materials Science and Engineering, Graduate School of Engineering, Osaka University, 2-1, Yamada-oka, Suita, Osaka 565-0871, Japan

e-mail: xwli@mat.eng.osaka-u.ac.jp and xwli69@hotmail.com

ABSTRACT

The dislocation arrangements induced by cyclic deformation in some differently oriented copper single crystals were investigated using electron channelling contrast (ECC) technique in scanning electron microscopy (SEM). It is shown that the ECC technique can well be used to examine dislocation arrangements in fatigued copper single crystals, especially at higher imposed plastic strain amplitudes. The typical dislocation structures in the cyclically deformed copper single crystals detected by this technique are in good agreement with those found by transmission electron microscopy (TEM). Furthermore, the SEM-ECC technique shows some attractive advantages compared to TEM. For instance, ECC observation clearly reveals an evolutional process of dislocation structure from the vein structure of matrix formed at lower strain amplitude to the labyrinth structure formed at higher strain amplitude. Moreover, the exact observations of dislocation arrangements within cyclic deformation bands (DBs), which are rather difficult to achieve by TEM, are successfully accomplished using the ECC method. The DBs formed in cyclically strained copper single crystals may exhibit quite different microstructures, depending upon their crystallographic orientation and accumulated plastic strain, such as PSB ladder, wall and labyrinth structures. Finally, combining the existing TEM results with the present SEM-ECC observations, we can state with certainty that the crystallographic orientation has a strong effect on the saturation dislocation features of copper single crystals.

1. INTRODUCTION

The electron channelling effect in scanning electron microscopy (SEM) was discovered in 1967 by Coates [1]. It was recognized that the electron channelling phenomenon results from large-angle inelastic scattering, i.e. back-scattering, of electron by phonons [2], and that the intensity of

back-scattered electrons depends strongly upon incident beam orientation with respect to the crystal lattice as well as dislocation density in the crystal. The principle for the phenomenon has been described in detail by Zauter et al. [3]. Stickler et al. [4] attempted for the first time to apply the electron channelling effect to the study of deformation behaviour of materials. Subsequently, Joy and Booker [5] achieved success in its application to the characterization of subgrains in deformed stainless steel.

Although the electron channelling contrast (ECC) technique was established over two decades ago and shown to be a powerful SEM technique for the qualitative and quantitative description of the dislocation arrangement on a mesoscopic scale, it has not found a wide application in the recent past, probably due to the limited resolution attainable by normal SEM. The more recently, however, some investigators [6-19] have reconsidered some of the attractive advantages of the ECC technique and utilized it to study deformed materials. Actually, in contrast to transmission electron microscopy (TEM), although the resolution attainable for ECC technique is only on the order of one tenth of a micron so that it cannot detect single defects that are too weak to image on SEM, its superiority in the research of materials should not be overlooked. For example, it allows observation of clusters of dislocation patterns over a much wider field of view, particularly at some special sites such as the vicinity of the grain boundary, crack tip and deformation band. It is also non-destructive technique, which enables one to explore the dislocation evolution at different stages of fatigue using a single specimen. For these reasons, the ECC technique has been well recognized recently and has stimulated an upsurge in research on imaging of dislocation arrangements induced by fatigue [8-19].

The cyclic deformation behaviour and dislocation structures of single-slip-oriented copper single crystals have been well documented in the last three decades [20-22]. Almost all kinds of dislocation structures of cyclically deformed copper single crystals were investigated previously by TEM, and the ECC technique has rarely been used in this field except by a very few researchers [12-15] who studied dislocation patterns in fatigued copper single crystals oriented for single slip or multiple slip. More recently, Li et al. [23-28] examined systematically the cyclic deformation behaviours of differently oriented copper single crystals and found that the crystallographic orientation has a strong effect on this behaviour of those crystals oriented for double slip or multiple slip [29-30]. The objective of this paper was to show the effect of such orientation on dislocation structures in cyclically deformed copper single crystals and the microstructure in deformation bands induced by cyclic deformation using the SEM-ECC imaging method. These studies are expected to provide complementary and new information not readily available by TEM.

2. EXPERIMENTAL PROCEDURES

All of the copper single crystals with $[\bar{1}35]$, $[\bar{5}\ 12\ 21]$ single-slip and $[\bar{1}12]$, $[017]$ double-slip orientations were grown from OFHC copper of 99.999% purity by the Czochralski or Bridgman technique. The orientation of the specimens was determined by the Laue back-reflection technique with an accuracy of within 2°. All the crystallographic orientations adopted for the present study are shown in the standard stereographic triangle as seen in Fig. 1. Before the fatigue tests, the
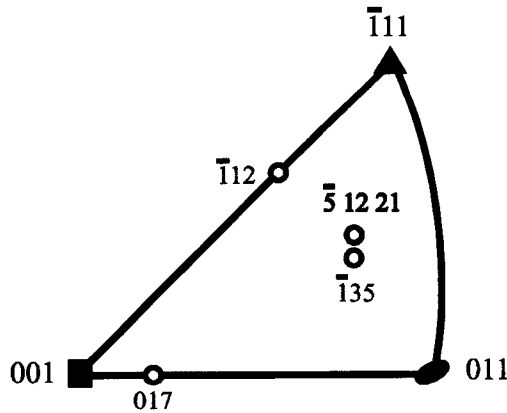
Fig. 1 Stereographic triangle showing the orientations of copper single crystals involved in this paper

specimens were carefully polished electrolytically to obtain a strain-free and mirror-like surface. Symmetrical push-pull fatigue tests were performed on servo-hydraulic testing machines at room temperature in air under plastic strain control. A triangular waveform signal with a frequency range of 0.05~0.5 Hz was employed. Cyclic stress-strain hysteresis loops were registered with an X-Y plotter, and the loop width ($\Delta\varepsilon_p$) at zero stress was kept constant during testing. The plastic resolved shear strain amplitude γ_{pl} and shear stress τ were calculated by $\gamma_{pl} = \Delta\varepsilon_p/2\Omega$ and $\tau = \sigma\Omega$,

where Ω is the Schmid factor of primary slip system and σ is an average value of the peak stresses in push and pull. For the $[\bar{5}\ 12\ 21]$ crystal specimen, the fatigue test was only performed at a higher plastic shear strain amplitude of 8.0×10^{-3} for 2×10^4 cycles to examine the microstructures in deformation bands. The other specimens were cycled until cyclic saturation.

One of the cyclically deformed specimen surfaces was polished mechanically and then electrolytically for observation of dislocation arrangements by SEM-ECC. A high-quality electro polishing is essential to obtain a better ECC image. The electro-polishing procedures adopted here are given in Table 1. The ECC technique was applied in a Cambridge S360 SEM using an inverted imaging mode. Dislocation-poor regions therefore appear as bright areas in the micrograph, whereas dislocation-dense regions are seen as dark fields; this is in accord with a TEM micrograph under bright imaging conditions. The parameters of SEM working conditions were carefully set at those listed in Table 2.

Table 1 The adopted electro-polishing procedures

Electro-polishing solution	Operating voltage	Operating current	Operating time
1000 ml of distilled water (H_2O) 500 ml of phosphoric acid (H_3PO_4) 500 ml of ethanol (C_2H_5OH) 100 ml of urea ($CH_3CH(OH)CH_3$) 10 g of 2-propanol (NH_2CONH_2)	8 V or so	3 A or so	3 – 4 minutes

Table 2 Parameters of the SEM working conditions

Acceleration voltage	Working distance	Filament	Probe	Brightness	Contrast	Scanning rate	Collector (V)
20 kV	15-22 mm	I = 2-3 A	I = 2-5 nA	80-95%	30-33%	$TV/2$ k	0

3. EXPERIMENTAL RESULTS AND DISCUSSION

3.1. Cyclic Stress-Strain (CSS) Behaviour

Fatigue testing conditions and data of cyclic hardening and saturation are listed in Table 3, where $\gamma_{pl, \, cum}$ ($\gamma_{pl, \, cum} = 4N\gamma_{pl}$, N is the total cyclic number) is the cumulative plastic strain, τ_s the saturation shear stress, τ_{max} the maximum shear stress, and τ_s/τ_{max} is a parameter describing cyclic softening behaviour.

Table 3 Fatigue testing conditions and data for differently oriented crystals

Orientation	Specimen No.	γ_{pl}	$\gamma_{pl, \, cum}$	τ_s	τ_{max}	τ_{max}/τ_s
$[\bar{1}35]$	S1	1.7×10^{-4}	18.2	28.0	29.0	1.03
	S2	6.6×10^{-4}	21.2	28.2	29.8	1.06
	S3	4.1×10^{-3}	48.0	28.4	29.5	1.03
	S4	6.0×10^{-3}	86.7	29.9	31.1	1.04
$[\bar{1}12]$	C1	3.7×10^{-4}	44.4	26.9	28.2	1.05
	C2	7.1×10^{-4}	62.5	28.7	31.5	1.10
	C3	2.3×10^{-3}	65.3	28.7	28.7	1.00
$[017]$	D1	1.2×10^{-4}	40.3	28.6	28.6	1.00
	D2	9.4×10^{-4}	90.2	37.1	39.6	1.07
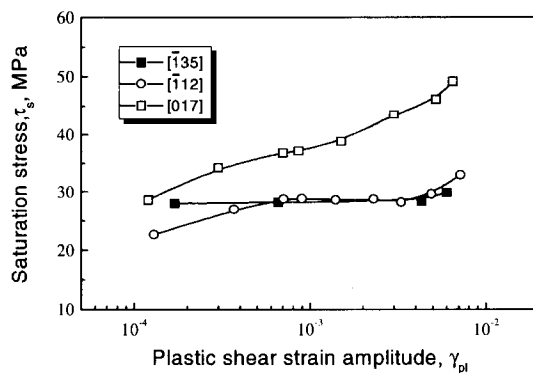
Fig. 2 The cyclic stress-strain curves of three differently oriented crystals

In Fig. 2 and Table 3 are shown the cyclic stress-strain (CSS) curves and the fatigue data of three differently oriented crystals. It can be seen that the $[\bar{1}35]$ single crystals present a saturation stress plateau over a shear strain range of 1.7 $\times$ 10^{-4} to 4.1 $\times$ 10^{-3}, and the saturation plateau stress is around 28.2 MPa, which is basically in agreement with the results reported by Mughrabi [31]. As strain increases above the plateau, the saturation stress rises to 29.9 MPa at γ_{pl} = 6.0 $\times$ 10^{-3}. In our previous work, the CSS curves of copper single crystals with different double slip orientations were well established [24-26]. Here, the CSS curves of $[\bar{1}12]$ and $[017]$ double-slip crystals are also given in Fig. 2. The curve of the $[\bar{1}12]$ crystal exhibits three distinctive regions and shows a clear plateau in the second region of 5.0 $\times$ $10^{-4} < \gamma_{pl} <$ 4.0 $\times$ 10^{-3} with an average saturation stress of 28.6 MPa, while the CSS curve of the $[017]$ crystal do not show a clear plateau, but a narrow quasi-plateau over the range of about 5.0 $\times$ $10^{-4} \sim$ 1.5 $\times$ 10^{-3}. The CSS behaviour for these two oriented crystals have been described in detail in Refs. [25, 26].

3.2. ECC Observation of the Saturation Dislocation Structure in $[\bar{1}35]$ Single-Slip Crystal

It is generally accepted based on the TEM observation that the three regions of the CSS curve correspond to different dislocation structures. In the plateau region, a dislocation feature can be described as well-known two-phase structure: the ladder structure of the persistent slip bands (PSBs) and the vein structure of the matrix [31-34]. The ladder structure is soft and carries most of the applied plastic strain, while the vein structure is hard and contributes little to cyclic straining. On the crystallographic plane $(1\bar{2}1)$, the matrix structure appears as loop patches, and the PSB appears as ladder structure, the average spacing of the rungs of the PSB ladder is 1.3 μm, and the thickness of the rungs is 0.1 ~ 0.2 μm. The dislocation structure consists only of veins at γ_{pl} below the plateau, and labyrinth and cell structures may develop above the plateau [34, 35].
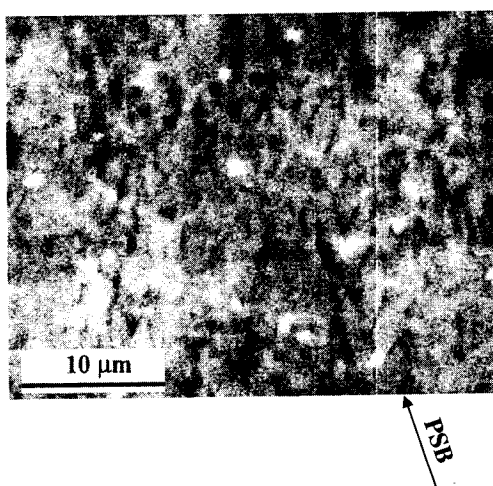

Fig. 3 SEM-ECC image of dislocation structures in $[\bar{1}35]$ crystal specimen S1 cycled at $\gamma_{pl} = 1.7 \times 10^{-4}$.

In the present study, the dislocation pattern of the cyclically saturated $[\bar{1}35]$ single crystal at different plastic strain amplitudes was observed by SEM-ECC. At the lowest strain amplitude γ_{pl} of 1.7×10^{-4} investigated, the low contrast of the ECC image does not permit a good showing of the dislocation structure, but the typical ladder structure is faintly visible as shown in Fig. 3. The lower contrast of the dislocation images at this strain amplitude seems to imply that the dislocation density in the PSB ladders is still lower. As the strain amplitude increases to 6.6×10^{-4}, ECC observation shows that the long straight PSB ladders are embedded in the loop patches of the matrix as shown in Fig. 4, where the observed plane is $(3\overline{26}15)$. These are in good agreement with the two-phase dislocation structure observed by TEM at the low strain amplitudes of the plateau region in the CSS curve [32]. Furthermore, the average spacing and thickness of the rungs in PSB ladders are evaluated to be about 1.4 μm and 0.1 ~ 0.2 μm, respectively; these values are also consistent with those obtained by TEM. In general, even though preparation of a thin-foil TEM sample is fairly successful, it is still difficult to obtain a clear TEM dislocation structure image over a much wider field of view (<2000x). However, it is quite easy to gain a clear low-magnification (~800x) dislocation structure image shown in Fig. 4 by using the ECC technique. Thus, the use of this technique may open up an opportunity for studying the macroscopic heterogeneity of the plastic deformation of materials, such as the dislocation features of macro-bands induced by cyclic deformation (see Section 3.6).

At the higher strain amplitude of the plateau region $(\gamma_{pl} = 4.1 \times 10^{-3})$, it was found that irregular PSB ladders (Fig. 5(a)) and labyrinth (Fig. 5(b)) form throughout the entire gauge section of the

specimen and become predominant, which provides supporting evidence that, strictly speaking, the plateau does not correspond only to the two-phase model described by Winter [32]. It can be noted from Fig. 5(a) that the ladder of PSB becomes irregular and is partially transformed into the cell structure. In addition, the vein structure of the matrix basically disappears and is superseded by a labyrinth that occurs over a wide area (Fig. 5(b)). The above results are quite similar to the work based on TEM by Ackermann et al. [36].
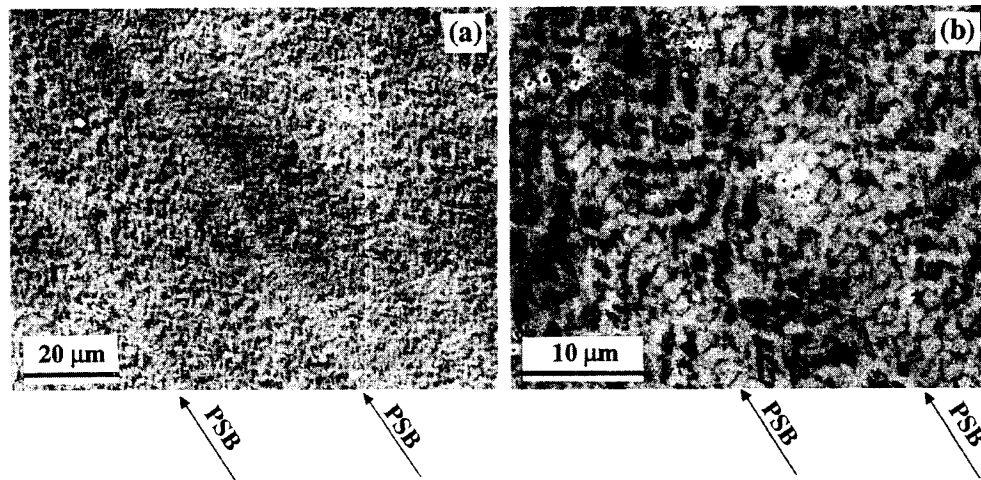
Fig. 4 SEM-ECC images of dislocation structures in the $[\overline{1}35]$ crystal specimen S2 cycled at $\gamma_{pl} = 6.6 \times 10^{-4}$. (a) low magnification and (b) high magnification
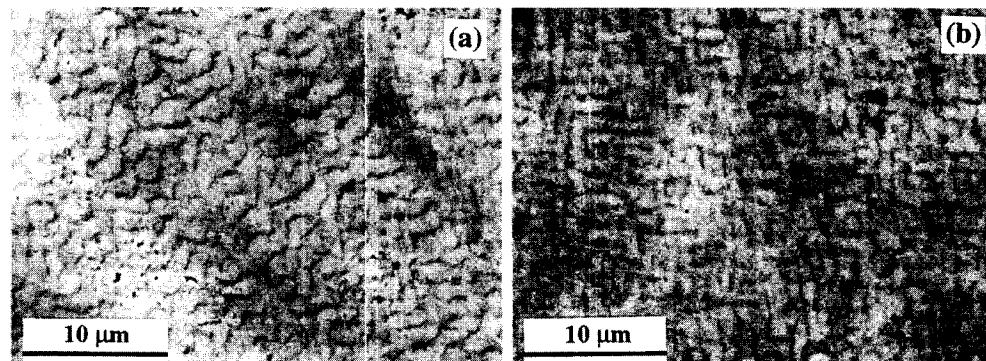
Fig. 5 SEM-ECC images of dislocation structures in the $[\overline{1}35]$ crystal specimen S3 cycled at $\gamma_{pl} = 4.1 \times 10^{-3}$. (a) irregular PSB ladders and (b) labyrinth

For the case of $\gamma_{pl} = 6.0 \times 10^{-3}$ above the plateau region, the dislocation arrangement is also found to consist primarily of a labyrinth and an irregular PSB ladder composed of cells (Fig. 6), resembling those formed at the higher strain amplitude of the plateau region ($\gamma_{pl} = 4.1 \times 10^{-3}$).
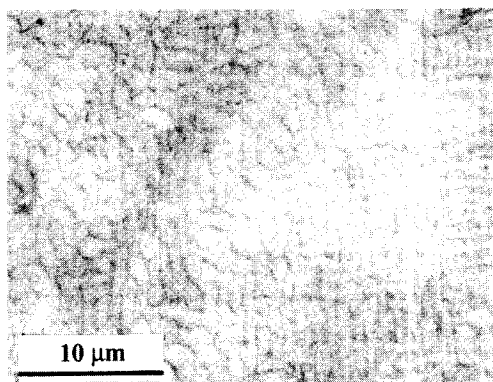
3.3. Relationship between Dislocation Microstructure and Crystallographic Slip Feature in [$\bar{1}$35] crystal

Fig. 6 SEM-ECC image of dislocation structures in [$\bar{1}$35] crystal specimen S4 cycled at $\gamma_{pl} = 6.0 \times 10^{-3}$.

After the saturation dislocation patterns were examined by ECC technique, additional cyclic numbers of 600 were imposed on specimens S2 and S4 at the corresponding strain amplitudes listed in Table 3. The deformation patterns of specimens S2 and S4 induced by 600 additional cycles were then further observed by the same method to reveal more distinctly the evolution of dislocation structure with increasing γ_{pl} and to clearly link well up the dislocation pattern with the crystallographic slip feature. Fig. 7(a) and (b) show the slip feature of PSBs and dislocation structures of matrix in specimens S2 and S4, respectively, after 600 additional cycles. As shown in Fig. 7(a), the dislocation pattern corresponding to PSBs cannot be seen without
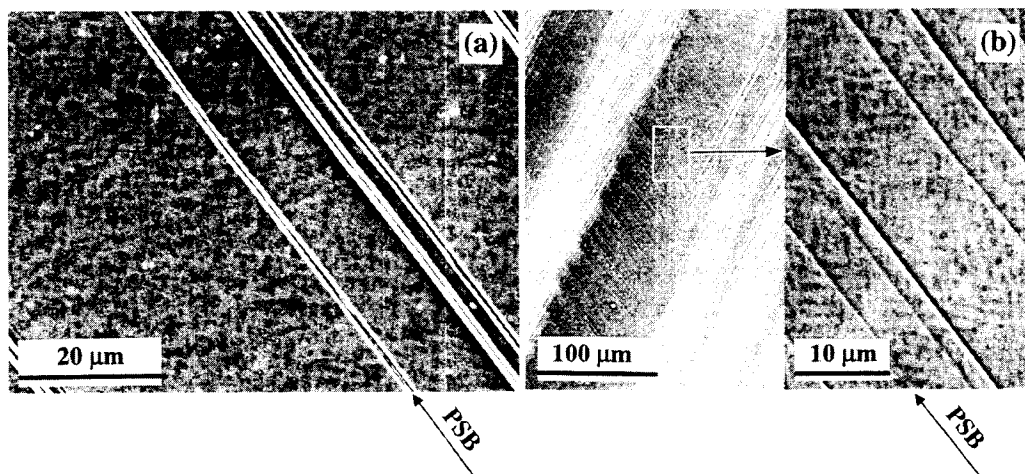

Fig. 7 SEM-ECC images of deformation patterns in specimen S2 and S4 cycled for 600 additional cycles under the corresponding strain amplitude.

(a) S2, $\gamma_{pl} = 6.0 \times 10^{-4}$ and (b) S4, $\gamma_{pl} = 6.0 \times 10^{-3}$

repolishing, except for the surface topology of these bands; however, the dislocation pattern of matrix, i.e. vein structure, is as seen clearly visible as that before additional cycling (Fig. 4). This is further evidence that PSBs are much softer than the vein structure of matrix and carry nearly the entire cyclic plastic deformation, which has been shown by other means [37]. The slip feature of PSBs shown in Fig. 7(a) appears to correspond well to the ladder structure in Fig. 4. Similarly, Fig.

7(b) implies that PSBs are also much softer than the labyrinth structure, although the formation of labyrinth structure can carry a part of the cyclic plastic deformation. From Fig. 7(a) and (b) it is clear that there exists an evolution of dislocation, i.e. the vein structure of matrix formed at lower amplitude is replaced by the labyrinth structure formed at higher amplitude.

3.4. ECC Observation of the Saturation Dislocation Structures in $[\bar{1}\,12]$ and [017] Double-Slip Crystals

Although fundamental invest- igations of the dislocation structure in cyclically deformed copper single crystals oriented for single slip have yielded a wealth of experimental results, there is as yet no general knowledge on the dislocation structure of double-slip-oriented copper single crystals produced in cyclic deformation [38-41]. Hence, much systematic work is needed to clarify the micro-mechanism of cyclic deformation in double-slip-oriented crystals. The work described here focuses on the dislocation structures of the cyclically saturated $[\bar{1}\,12]$ and [017] double-slip crystals observed using the ECC technique.

Fig. 8 presents the dislocation structures in the $[\bar{1}\,12]$ crystals cyclically strained at different plastic strain amplitudes. In Fig. 2 the CSS curve of the $[\bar{1}\,12]$ crystal exhibits a clear plateau over the strain range of about $5.0 \times 10^{-4} \sim 4.0 \times 10^{-3}$. Winter [32] proposed a two-phase model to account for the existence of the plateau region in this curve for single-slip crystals. The formation of PSB ladders is now generally considered the main reason for the occurrence of the plateau. As shown in Fig. 8(b) and (C), the well-developed PSB ladder structures form at 7.1×10^{-4} and 2.3×10^{-3}, which fall respectively in the lower end and middle of the plateau in the CSS curve of the $[\bar{1}\,12]$ crystal. Jin and Winter [39] also reported two separated sets of PSB structures in a $[\bar{1}\,12]$ crystal cyclically deformed at a plastic strain amplitude of 3.0×10^{-3} exactly within the plateau region. These results provide powerful evidence that occurrence of the plateau region in the CSS curve of $[\bar{1}\,12]$ crystal is probably attributable to the formation of PSB ladder structures, which is quite similar to the case for single-slip crystals. However, it is very interesting to note from Fig. 8(a) that PSB ladder structures occur even in the lower strain amplitude of 3.7×10^{-4} below the plateau region in CSS curve for the $[\bar{1}\,12]$ crystal. This result is greatly different from the previous ones obtained with single-slip crystals [31], for which PSBs form only in the plateau region in CSS curve. In the recent work [42], we detected systematically the changes of hysteresis loop shape parameter V_H with number of cycles N in the $[\bar{1}\,12]$ copper single crystals during cyclic deformation. It was found that, when the strain amplitude γ_{pl} is even below the plateau region in CSS curve (*e.g.* γ_{pl} = 3.7×10^{-4}), the curve of $V_H - N$ shows obvious minimum, implying the possible formation of PSBs in these lower strain ranges in terms of the definition of V_H [31, 42, 43]. The present results based on ECC observation are in good agreement with the V_H analysis. However, it deserves to be mentioned that the PSB ladder structures (Fig. 8(a)) are just in the initial stage of formation and are not well developed when the applied strain amplitude is below the plateau region in CSS curve. As it is well known, if the applied strain amplitude is in excess of a certain value, the transformation from the matrix vein structure to the PSB ladder structure must take place to accommodate high values of plastic strains. Winter [44] suggested that this transformation occurs at the soft centres of
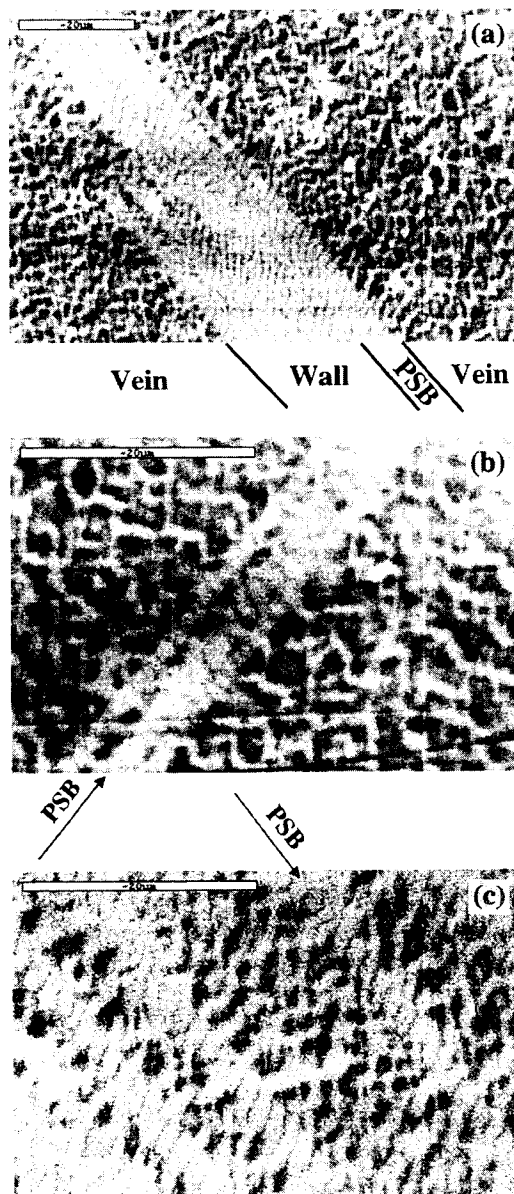
Fig. 8 SEM-ECC images of dislocation structures in the [$\bar{1}$ 12] crystals cycled at different strain amplitudes.
(a) $\gamma_{pl} = 3.7 \times 10^{-4}$, (b) $\gamma_{pl} = 7.1 \times 10^{-4}$ and (c) $\gamma_{pl} = 2.3 \times 10^{-3}$.

veins wherein exist small dislocation-poor areas surrounded by a harder vein shell of higher dislocation density, and then the surviving vein shell segments develop the first dislocation walls. Subsequently, the walls shift at a certain rate with cycling and gradually form the typical ladder pattern in the PSBs. These results are based only on single-slip-oriented copper single crystals; however, whether and how such a transformation would happen in cyclically deformed copper single crystals oriented for double slip was not reported. In the present study, it can be perceived from Fig. 8(a) that there exists an obvious transition region (i.e. walls) in the process of the transformation from the vein structure to the PSB ladder structure, which is essentially similar to the case for single-slip crystals. Nevertheless, the main distinction is that the transformation occurs only in the plateau regime for single-slip crystals, whereas the transformation can occur even below the plateau regime for the [$\bar{1}$ 12] crystal, and the PSB ladder structure and the transitional wall structure coexist. Such difference is believed to be associated with different geometrical relationships between crystal orientations and corresponding slip systems for these oriented crystals.

Fig. 9 shows the dislocation structures in the [017] crystals cycled at different plastic strain amplitudes. At lower strain amplitude of 1.2×10^{-4}, these structures are basically composed of irregular labyrinth structures as shown in Fig. 9(a). The widths of channels are determined roughly to be 0.8 ~ 1.3 μm. As the imposed amplitude increases to 9.4×10^{-4} within the quasi-plateau region in the CSS curve, the major area is covered by regular

labyrinth structures, and the average width of channels is reduced to ~0.5 μm. We also note that some narrow PSB ladder-like structures are embedded in the labyrinth structures, seemingly forming a distinctive two-phase structure, i.e. labyrinth structure of the matrix and PSB ladder-like structure, which is somewhat different from the two-phase structure obtained with single-slip crystals over the plateau region in the CSS curve. Gong et al. [45, 46] found a quite similar structure in cyclically deformed [001] multiple-slip-oriented copper single crystals; however, they called the ladder-like structure "strip" -like structure, which occupies a very small volume fraction (< 5% at $\gamma_{pl} = 1.8 \times 10^{-3}$), while in the [017] crystal such a ladder-like structure accounts for a much greater volume fraction (see Fig. 9(b)). Wang et al. [46] speculated that the increase in the scale of the labyrinth structure with decreasing applied strain amplitude is one of the main reasons for the complete disappearance of a plateau region in the CSS curve of the [001] crystal. Although the scale of the labyrinth structure increases with decreasing strain amplitude, the CSS curve of the [017] crystal still shows a narrow quasi-plateau region primarily due to the formation of PSB ladder-like structures, which carry a considerable part of the cyclic plastic strain. For the [017] critical double-slip crystal, the formation of ladder-like structures might be promoted by the involvement of a critical (secondary) slip [40]. According to the analyses above it is reasonable to conclude that the occurrence of a quasi-plateau region in the CSS curve of the [017] crystal results from the joint effects of the scale change of the labyrinth structure and the formation of PSB ladder-like structures.
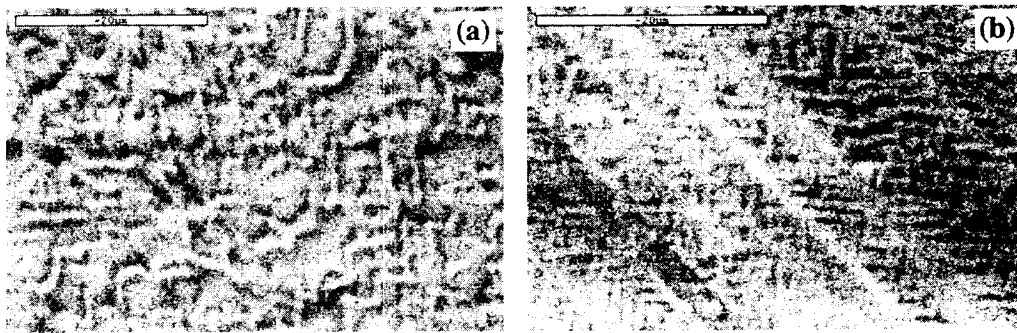

Fig. 9 SEM-ECC images of dislocation structures in the [017] crystals cycled at different strain amplitudes. (a) $\gamma_{pl} = 1.2 \times 10^{-4}$ and (b) $\gamma_{pl} = 9.4 \times 10^{-4}$.

3.5. Orientation Dependence of Cyclic Saturation Dislocation Structures of Copper Single Crystals

In our previous work the orientation dependence of the plateau behaviour in the CSS curve of copper single crystals was well summarized [29]. For comparison, the orientation dependence of cyclic saturation dislocation structures of copper single crystals is also summarized schematically in Fig. 10 by combining the existing TEM results with the present SEM-ECC observations. It is interesting to note in the figure that the saturation dislocation structures change regularly with the variation in crystallographic orientation. For example, for the crystals located on the [011]-[001] or [011]-[$\bar{1}$11] side of the standard stereographic triangle, the dislocation structures change generally from PSB ladder structures to labyrinth structures or cell structures, respectively, when the

orientation varies from the [011] orientation to the [001] orientation or to the $[\bar{1}11]$ orientation. However, for the crystals located on the $[001]\text{-}[\bar{1}11]$ side, PSB ladder structures obviously form in the $[\bar{1}12]$ crystal, while PSB ladder structures for the crystals located on both sides of a $[\bar{1}12]$ crystal tend to die out and evolve as labyrinth structures or cell structures when the orientation varies from the $[\bar{1}12]$ orientation to the [001] orientation or to the $[\bar{1}11]$ orientation, respectively. Such an orientation dependence of cyclic saturation dislocation structure provides a good account for the orientation dependence of the plateau behaviour in the CSS curve of copper single crystals.

Fig. 10 Standard stereographic triangle showing the variation of saturation dislocation structures with crystallographic orientation. The references relevant to experimental results by individual investigators are also given in brackets.

3.6. ECC Observation of the Dislocation Microstructure in Deformation Bands (DBs)

Besides the general slip bands and the well-known persistent slip bands (PSBs), deformation bands (DBs) occur often as an important surface deformation mode in a single crystal subjected to cyclic straining. The formation of DBs in fatigued crystals is a kind of grievous damage that may influence the nucleation and propagation of fatigue cracks [49]. Accordingly, a clear understanding of the formation mechanism of DBs is of particular importance, and undoubtedly knowledge of the dislocation microstructure of DBs is an essential prerequisite. Although some investigators [31, 49-52] have examined the macroscopic behaviour of DBs in some cyclically deformed copper

single crystals, due to the difficulty in experimental technique, observation of the microstructures in DBs has still not been successful. Recently Gong et al. [13] used the SEM-ECC technique to detect the dislocation microstructures in DBs formed in cyclically deformed [001] multiple-slip copper single crystals. They found that the DBs contain labyrinth structures plus strips, whereas the areas between DBs contain exclusively the (001) dislocation wall structures. In the present paper, the dislocation microstructures in DBs formed in cyclically deformed single-slip copper single crystals at higher strain amplitudes were revealed using the SEM-ECC technique.
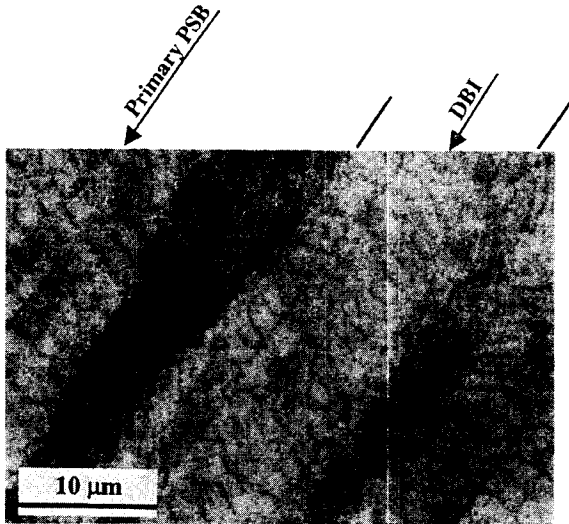
Fig. 11 SEM-ECC image of dislocation structures in DBI in a [$\bar{1}$35] single-slip copper single crystal cyclically deformed at γ_{pl} = 6.0 × 10⁻³. (Note that DBI develops almost along the primary PSBs)

Two types of deformation band denoted DBI and DBII have often been observed in cyclically deformed copper single crystals with various orientations [23-26, 52]. DBI develops almost along the primary PSBs while DBII makes a certain angle with the primary PSBs. The macroscopic characteristics of the two kinds of DBs were discussed systematically in a previous paper [53]. Fig. 11 gives the dislocation structure in the DBI-type deformation band formed in cyclically deformed [$\bar{1}$35] copper single crystal at a higher strain amplitude of 6.0 × 10⁻³. It can be seen that the dislocation structure relevant to DBI consists of irregular PSB ladder structures, and the surrounding matrix consists of dislocation wall or labyrinth structures. Fig. 12 shows the microstructures of the DBII-type deformation band and the adjacent regions in a [$\bar{5}$ 12 21] crystal cycled at higher strain amplitude of 8.0×10⁻³ for 2×10⁴ cycles. It is clear from Fig. 12(a) that DBII makes a certain angle with the primary PSBs and has a clear boundary with the surrounding regions. Further observations show that the microstructures within DBII are entirely composed of parallel PSB ladders as shown in Fig. 12(b), while the microstructures of the matrix consist of narrow slip bands and irregular veins. Deformation bands are thought to be areas of plastic strain accumulation, and the dislocation structure relevant to DBs would correspond to the structure that is more capable of carrying large plastic strain. For the [001] multiple-slip crystal, since the plastic strain is mainly carried by labyrinth structures [46], the dislocation structure in DBs consists primarily of labyrinth structures. On the other hand, the soft PSB ladder structures, which carry the majority of the plastic strain, can form easily in cyclically deformed [$\bar{1}$35] and [$\bar{5}$ 12 21] single-slip crystals; so the dislocation structure in DBs (DBI or DBII) primarily consists of PSB ladder structures for the [$\bar{1}$35] and [$\bar{5}$ 12 21] crystals.
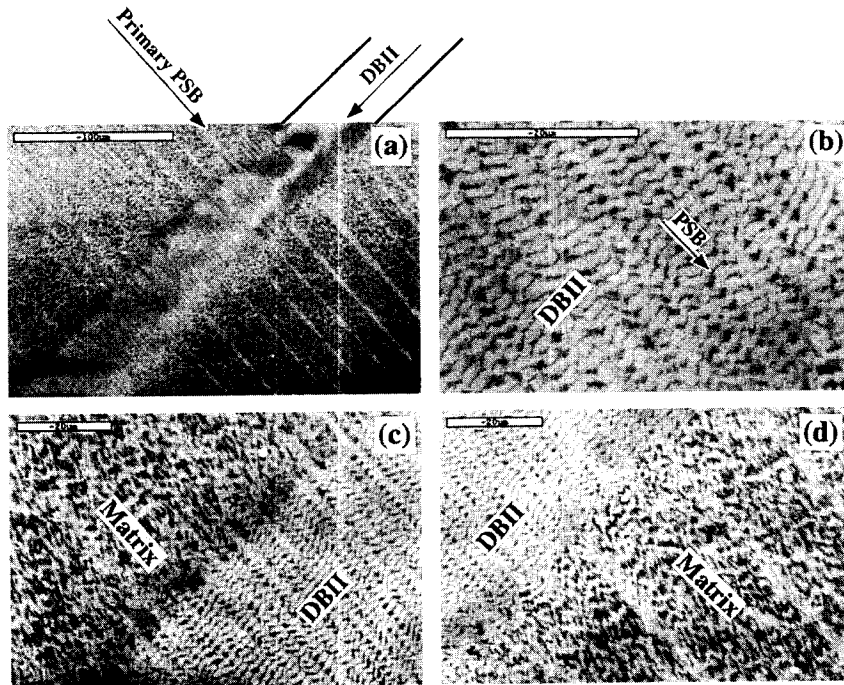
Fig. 12 SEM-ECC images of dislocation arrangements in DBII in a $[\bar{5}\ 12\ 21]$ single-slip copper single crystal cyclically deformed at $\gamma_{pl} = 8.0 \times 10^{-3}$ for 2×10^4. (a) full view of DBII and the surrounding matrix; (b)dislocation arrangements within DBII and (c), (d) dislocation arrangements near the boundary of DBII. (Note that DBII makes a certain angle with the primary PSBs)
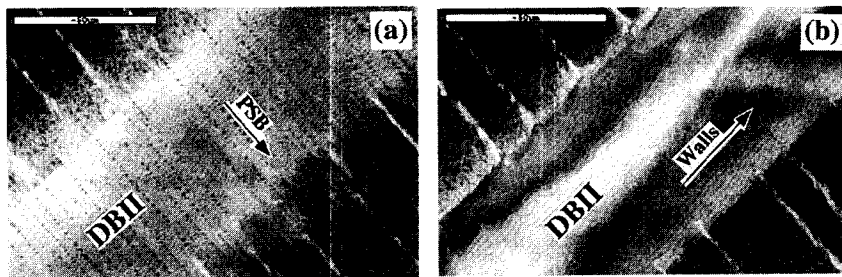

Fig. 13 SEM-ECC images showing different dislocation structures in DBII in the same a $[\bar{5}\ 12\ 21]$ single-slip copper single crystal cyclically deformed at $\gamma_{pl} = 8.0 \times 10^{-3}$ for 2×10^4. (a) DBII featuring PSB ladder structures and (b) DBII featuring wall structures.

In addition, it is quite interesting to find that the dislocation arrangements within a deformation band (DB) formed in the identical $[\bar{5}\ 12\ 21]$ crystal cycled under the same applied conditions may exhibit different features, as shown in Fig. 13. The microstructure within the DBII in Fig. 13(b) apparently consists of typical wall structures rather than the PSB ladder structures in Fig. 13(a).

There is no doubt that the formation of DBs results from deformation localization in crystal and takes place successively over different regions of the crystal. When the imposed cumulative strain carried by some preferably formed DBs reaches a certain capacity, the microstructures in these DBs may transform from PSB ladder structures into more stable wall structures. We can thus regard the DB in Fig. 13(b) as being well-developed, so that should be steady in energy. At the same time, one can note that those dislocation walls in the well-developed DB are not perfectly parallel, which might be associated with the crystal rotation within the DB, further indicating a serious local plastic deformation concentration within such a DB.

In summary, the DBs formed in cyclic straining of copper single crystals can exhibit quite different microstructures, depending upon the crystallographic orientation, the accumulated plastic strain and so on. Undoubtedly, such deformation macro-bands formed in cyclic deformation would act as a soft phase to accommodate much more plastic strain, thus resulting in the initiation and propagation of fatigue cracks along those DBs.

4. CONCLUDING REMARKS

With the discovery of the electron channelling effect in SEM, the electron channelling contrast technique has in recent years emerged as a powerful SEM means of investigating of deformed materials, especially of metal crystal materials. In this paper, dislocation arrangements in cyclically deformed copper single crystals with different crystallographic orientations were investigated and summarized in a relatively systematic way. The SEM-ECC technique was shown able to image easily dislocation arrangements in fatigued copper single crystals with different crystallographic orientations. The typical dislocation structures in the cyclically deformed copper single crystals achieved by this method are in good agreement with those observed by TEM. Combined with some existing TEM results, ECC observations give qualitatively an orientation dependence of cyclic saturation dislocation structure of copper single crystals, which accounts well for the orientation dependence of the plateau behaviour in the CSS curve of copper single crystals. By establishing the relationship between dislocation microstructure and crystallographic slip feature, ECC observation clearly reveals an evolutional process of dislocation from the vein structure to the labyrinth structure with an increase in applied strain amplitude. The careful ECC observation of dislocation arrangements within deformation bands show that the DBs formed in cyclically strained copper single crystals may exhibit quite different features, depending upon the crystallographic orientation and the accumulated plastic strain.

Finally, we want to point out that, because it is possible with the ECC technique to observe dislocation arrangements generated during cyclic deformation without destroying the specimen, this means can be successfully employed to investigate the evolutional rule of dislocation structures with varying cumulative plastic strain or applied plastic strain amplitude. Ma and Laird [54, 55] attempted to determine the evolutional rule of dislocation structures in copper single crystals under variable loading by TEM. However, the crystal specimen must be sectioned for TEM examination so that the fixed observation of the process of dislocation evolution cannot be achieved relying only

on this means; this results in inconclusive experimental results. On the contrary, the ECC experimental results are just based on the same crystal specimen, but it need not be destroyed during testing. The credibility of experimental results is thus greatly enhanced. For example, to investigate the evolutional rule of dislocation structures with varying cumulative plastic strain, the identical crystal specimen can be adopted for fatigue testing under a certain plastic strain amplitude control. At different stages of cycling, the testing will be stopped and the specimen is removed from the testing machine. So the dislocation structures corresponding to different stages of cycling can be observed on a certain fixed region of crystal surface using the ECC technique. By alternating the orientation of specimen and repeating the above testing, we can obtain the orientation dependence of the evolutional rule of dislocation structures. Similarly, we can investigate the effect of strain interaction (or load interaction) [54, 55] on the evolutional rule of dislocation structures. A systematic experimental effort is needed for these studies.

In a word, the studies above can be expected to achieve some new advances in the mesoscopic and microscopic field of crystallography of fatigue and fracture, and hence provide a solid foundation for researchers to further understand the cyclic deformation micro-mechanism of polycrystalline materials.

ACKNOWLEDGEMENTS

REFERENCES

1. D.G. Coates, Phil. Mag., **16** (1967), p. 1179

2. J.P. Spencer and C.J. Humphreys, Phil, Mag. B, **42** (1980), p. 433

3. R. Zauter, F. Petry, M. Bayerlein, C. Sommer, H.-J. Christ and H. Mughrabi, Phil. Mag. A, **66** (1992), p. 425

4. R. Stickler, C.W. Hughes and G.R. Booker, Proc. Of the 4th Annual Scanning Electron Microscopy Symposium, Chicago,IIT Research Institute, (1971), p. 473

5. D.C. Joy and G.R. Booker, Proc. Of the 6th Annual Scanning Electron Microscopy Symposium, Chicago,IIT Research Institute, (1973), p. 138

6. J.T. Czernuszka, N.J. Long, E.D. Boyes and P.B. Hirsch, Phil. Mag. Lett., **62** (1990), p. 227

7. A.J. Wilkinson and P.B. Hirsch, Phil. Mag. A, **72** (1995), p. 81

8. A.J. Wilkinson, M.B. Henderson and J.W. Martin, Phil. Mag. Lett., **74** (1996), p. 145

9. A. Schwab, J. Bretschneider, C. Buque, C. Blochwitz and C. Holste, Phil. Mag. Lett., **74** (1996), p. 449

10. D.L. Chen, D. Melisova, B. Weiss and R. Stickler, Fat. Fract. Engng. Mater. Struct., **20** (1997), p. 1551

11. J. Bretschneider, C. Holste and B. Tippelt, Acta Mater., **45** (1997), 3775

12. D. Melisova, B. Weiss and R. Stickler, Scripta Mater., **36** (1997), p. 1061

13. B. Gong, Z.R. Wang, D.L. Chen and Z.G. Wang, Scripta Mater., **37** (1997), p. 1605

14. J. Ahmed, A.J. Wilkinson and S.G. Roberts, Phil. Mag. Lett., **76** (1997), p. 237

15. X.W. Li, Y.M. Hu and Z.G. Wang, Mater. Sci. Eng, **A248** (1998), p. 299

16. Z.F. Zhang, X.W. Li, H.H. Su and Z.G. Wang, J. Mater. Sci. Technol., **14** (1998), p. 211

17. W.P. Jia, S.X. Li, Z.G. Wang, X.W. Li and G.Y. Li, Acta Mater., **47** (1999), p. 2165

18. Z.F. Zhang and Z.G. Wang, Phil. Mag. Lett., **80** (2000), 483

19. Z. F. Zhang and Z.G. Wang and S.X. Li, Phil. Mag. Lett., **80** (2000), p. 525

20. C. Laird, P. Charsley and H. Mughrabi, Mater. Sci. Eng. A, **81** (1986), p. 433

21. Z.S. Basinski and S.J. Basinski, Prog. Mater. Sci., **36** (1992), p. 89

22. S. Suresh, Fatigue of Materials, Cambridge University Press, London, 1998

23. X.W. Li, Z.G. Wang, G.Y. Li, S.D. Wu and S.X. Li, Acta Mater., **46** (1998), p. 4497

24. X.W. Li, Z.G. Wang and S.X. Li, Mater. Sci. Eng., **A260** (1999), p. 132

25. X.W. Li, Z.G. Wang and S.X. Li, Mater. Sci. Eng., **A265** (1999), p. 18

26. X.W. Li, Z.G. Wang and S.X. Li, Mater. Sci. Eng., **A269** (1999), p. 166

27. X.W. Li, Z.G. Wang and S.X. Li, J. Mater. Sci. Lett., **18** (1999), p. 1533

28. X.W. Li, W.P. Jia, Z.G. Wang and S.X. Li, J. Mater. Sci. Lett., **19** (2000), p. 641

29. X.W. Li, Z.G. Wang and S.X. Li, Phil. Mag. Lett., **79** (1999), p. 715

30. X.W. Li, Z.G. Wang and S.X. Li, Phil. Mag. Lett., **79** (1999), p. 869

31. H. Mughrabi, Mater. Sci. Eng., **33** (1978), p. 207

32. A.T. Winter, Phil. Mag., **30** (1974), p. 719

33. J.M. Finney and C. Laird, Phil. Mag., **31** (1975), p. 339

34. C. Laird, Dislocations in Solid, ed. By F.R.N. Nabarro, North Holland, **6** (1983), p. 1

35. N.Y. Jin and A.T. Winter, Acta Metall., **32** (1984), p. 1173

36. F. Ackermann, L.P. Kubin, J. Lepinoux, H. Mughrabi, Acta Metall., **32** (1984), p. 715

37. O. Helgeland, J. Inst. Met., **93** (1965), p. 570

38. N.Y. Jin, Phil. Mag., **A48** (1983), p. L33

39. N.Y. Jin and A.T. Winter, Acta Metall., **32** (1984), p. 989

40. B. Gong, Z.R. Wang, Z.G. Wang and Y.W. Zhang, Mater. Sci. Eng., **A210** (1996), p. 94

41. Y.W. Zhang, Master' s Thesis, Institute of Metal Research, Chinese Academy of Sciences, (1995).

42. X.W. Li, Z.G. Wang and S.X. Li, Mater. Sci. Eng., **A271** (1999), p. 315

43. J. Polak, J. Helesic and K. Obrlik, Mater. Sci. Eng., **A101** (1988), p. 7

44. A.T. Winter, Phil. Mag. **37** (1978), p. 457

45. B. Gong, Z.R. Wang and Z.G. Wang, Acta Mater., **45** (1997), p. 1365

46. Z.R. Wang, B. Gong and Z.G. Wang, Acta Mater., **45** (1997), p. 1379

47. N.Y. Jin, Phil. Mag. Lett., **56** (1987), p. 23

48. T.K. Lepisto, V.T. Kuokkala and P.O. Kettunen, Mater. Sci. Eng., **81** (1986), p. 457

49. M. Saletore and R. Taggart, Mater. Sci. Eng., **36** (1978), p. 259

50. C.R. Gostelow, Met. Sci. J., **5** (1971), p. 117

51. S.X. Li, B. Gong and Z.G. Wang, Scripta Metall. Mater., **31** (1994), p. 1729

52. B. Gong, Z.G. Wang and Y.W. Zhang, Mater. Sci. Eng., **A149** (1995), p. 171

53. X.W. Li, Z.G. Wang and S.X. Li, Phil. Mag. A., **80** (2000), p. 1901

54. B.T. Ma and C. Laird, Mater. Sci. Eng., **102** (1988), p. 247

55. B.T. Ma and C. Laird, Acta Metall., **37** (1989), p. 357